Corrosion Science 149 (2019) 123–132

Contents lists available at ScienceDirect

Corrosion Science

journal homepage: www.elsevier.com/locate/corsci

Influence of Al content and pre-oxidation on the aqueous corrosion resistance of binary Fe-Al alloys in sulphuric acid

Jian Peng[a,*], Frank Moszner[b], Julian Rechmann[a], Dirk Vogel[a], Martin Palm[a], Michael Rohwerder[a]

[a] Max-Planck Institut für Eisenforschung GmbH, Max-Planck-Str. 1, 40237 Düsseldorf, Germany
[b] Winterthur Gas & Diesel Ltd., Schützenstrasse 1-3, 8401 Winterthur, Switzerland

ARTICLE INFO

Keywords:
Fe-Al alloys
Aqueous corrosion resistance
Pre-oxidation
Sulphuric acid

ABSTRACT

The influence of Al content and pre-oxidation on the corrosion behavior of binary Fe-Al alloys in 0.0126 M H_2SO_4 was investigated. The minimum Al content for forming a passive film on binary Fe-Al at 25 °C is 15 at.% and passivation improves up to 25 at.% Al. X-ray photoelectron spectroscopy measurements show that the passive film on Fe-25Al is enriched in Al and consists of an outer layer of mixed Al and Fe hydroxides and an inner layer of Al oxide. The oxide layer generated at 1000 °C effectively protected against aqueous corrosion in H_2SO_4.

1. Introduction

Fe-Al-based alloys attract much attention for high temperature structural applications because of their outstanding properties. They exhibit a lower density of 5.7–6.7 g/cm^3 compared to other iron-based materials such as cast iron and stainless steels, superior high-temperature corrosion resistance, good wear resistance and low material costs [1–3]. In addition, the equipment for their production and processing is readily available in industry [2]. Fe-Al-based alloys are mainly developed for high-temperature structural applications [4,5]. However, due to their lower costs, they are also considered as a potential alternative for replacing conventional stainless steels at low temperatures. Applications that have been looked at in detail are pipes and tubes for sea water desalination [6], Cr- and Ni-free parts used in food industry [7], high-performance brake materials for trucks [8] and as catalysts [9]. For such applications, understanding of the aqueous corrosion behavior is of great importance.

A number of studies on the aqueous corrosion behavior of binary Fe-Al alloys have been reported so far, but they mainly focused on binary Fe-Al alloys with a limited variation of the Al content [10–26] or Fe-Al alloys with additional alloying elements [11,27–45]. Moreover, these investigations were carried out in a variety of electrolytes. Only two investigations were carried out using H_2SO_4 of low molarity. Masahashi et al. [46] investigated Fe-Al alloys with a wider range of Al content (5, 10, 15, 25 and 30 at.%). However, only the mass changes of the samples after immersion in 5×10^{-3} M H_2SO_4 at 40–100 °C up to 3 h were determined and corroded samples were inspected by scanning electron microscopy (SEM) and evaluated by X-ray photoelectron spectroscopy (XPS). The passivation behavior was not studied. A more extensive study was carried out by Chiang et al. [47] who investigated the passivation behavior of six Fe-Al alloys with Al contents between 3.4–41.7 at.% at 25 °C. However, no post mortem examinations were performed. Table 1 summarizes the compositions of the binary Fe-Al alloys and electrolytes investigated in previous investigations [10–14,16,11–26,34,46,47]. In summary, it has been recently concluded that a systematic study of the aqueous corrosion behavior of binary Fe-Al alloys is still necessary [13].

In general, it has been found that alloying Fe with Al leads to passivation in acid sulfate solutions [33,48]. Passivation and re-passivation improve with increasing Al content [48] and about 10 at.% Al are necessary to form a passive film and about 19 at.% Al are needed to exhibit a good aqueous corrosion resistance [47].

Whether formation of an Al_2O_3 scale through pre-oxidation, which effectively enhances the corrosion resistance of Fe-Al in gaseous environments [49–51] also has a beneficial effect during aqueous corrosion is not clear [48]. Buchanan and Perrin [43] pre-oxidized three highly alloyed iron aluminides at 1000 °C for 24 h and then tested their aqueous corrosion behavior in a mild acid chloride solution (H_2SO_4

* Corresponding author.
E-mail address: j.peng@mpie.de (J. Peng).

https://doi.org/10.1016/j.corsci.2018.12.040
Received 18 June 2018; Received in revised form 8 November 2018; Accepted 28 December 2018
Available online 02 January 2019

Table 1
Compositions of binary Fe-Al alloys and electrolytes investigated in previous works.

Alloys (in at.%)	Electrolytes	Ref.
Fe-(4-22)Al	0.5 M Na_2SO_4 + 6×10^{-5} M H_2SO_4	[19]
	0.1 M phthalate buffer (pH 5)	
Fe-6Al	0.5 M H_2SO_4	[18]
Fe-(8-22)Al	0.1 M phthalate buffer (pH 5)	[16]
	0.1 M borate buffer (pH 9.3)	[17]
	0.005 M H_2SO_4/0.5 M Na_2SO_4 (pH 2.5, pH 3.8)	
	1 M NaOH (0.631 M)	
Fe-22Al	0.5 M H_2SO_4	[23]
Fe-25Al	H_2SO_4 (5×10^{-5} M), NaOH (0.631 M)	[15]
	0.25 M H_2SO_4	[24]
	(0.11 M H_3BO_3 + 0.022 M $Na_2B_4O_7$, pH 8.4) with and without 100 mM KCl	[14]
	0.5 M H_2SO_4	[25]
Fe-26Al	0.25 M H_2SO_4	[13]
	0.5 M H_2SO_4	[26]
Fe-28Al	0.05 M H_2SO_4	[12]
	1 M H_2SO_4, 1 M Na_2SO_4, and 1 M NaOH	[11]
Fe-31Al	Simulated acid rain (pH 2.3)	[22]
Fe-34Al	Seawater with $Ca(OH)_2$, pH = 10, 12 and 14	[10]
Fe-40Al	0.5 M H_2SO_4	[20]
	NaOH + H_2SO_4, pH = 3, 7 and 11	[21]
Fe-45Al	Simulated acid rain (pH 2.3)	[22]
Fe-(5-30)Al	0.005 M H_2SO_4	[46]
Fe-(3.4-41.7)Al	0.05 M H_2SO_4	[47]

(5×10^{-5} M) + 200 ppm Cl-) and in a more aggressive sodium tetrathionate solution (0.001 M $Na_2S_4O_6$). Compared to the Fe-Al alloys with carefully cleaned surfaces, the oxidized alloys showed a much reduced resistance against pitting corrosion in the mild acid chloride solution and active corrosion was observed for alloys with and without pre-oxidation in the sodium tetrathionate solution [43]. Escudero et al. [45] investigated the aqueous corrosion resistance of a highly alloyed Fe-Al sheet strengthened by oxides in Hank's solution after pre-oxidation at 900 or 1100 °C for 3, 100 and 200 h. Though they found a good corrosion resistance after pre-oxidation, this was considered as not being perfect, because no continuous oxide scale formed. Strong local pitting was observed where large oxides in the microstructure of the Fe-Al sheet had retained the formation of an Al_2O_3 scale [45]. Lopez and Escudero [44] also tested two highly alloyed iron aluminides - one additionally oxide-dispersion strengthened (ODS) - in a mixed solution of NaCl, KCl and $CaCl_2$ of pH 7.4 for up to 14 days after pre-oxidation at 1100 °C for 2 h. They concluded that the tested alloys did not show a satisfactory corrosion behavior in the Cl- containing solution and that the corrosion resistance was not improved by generating an alumina layer through pre-oxidation [44]. No data are yet available for the effect on pre-oxidation on the aqueous corrosion of binary Fe-Al alloys.

In the present work, a systematic investigation of the influence of Al content up to 40 at.% on the corrosion resistance of binary Fe-Al alloys was performed. The passive film structure on Fe-25 at.% Al alloy was investigated. In addition, the aqueous corrosion behavior of a pre-oxidized Fe-25 at.% Al alloy was evaluated.

2. Experimental procedure

Binary Fe-*x*Al alloys (x = 5, 10, 15, 25, 30 and 40, in at.%) were prepared by induction melting under argon atmosphere (99.999%). Fe of 99.99% purity and Al of 99.999% purity were used as starting materials. Melts were cast into a cylindrical copper mould of 30 mm in diameter and about 200 mm in length. Wet-chemical analysis was conducted to check the composition of the alloys and the resulting values agreed well with the nominal compositions, generally within ± 0.5 at.%. Typical impurity contents of these alloys are C = 44 wt. ppm, N = 18 wt. ppm, O = 49 wt. ppm, Si < 10 wt. ppm, P < 20 wt. ppm, and S = 4 wt. ppm. The as-cast alloys were cut variously parallel or perpendicular to the casting direction into specimens with dimension of 10 mm in diameter and 2 mm in thickness by electrical discharge machining. The specimens were ground with emery papers up to P4000. Specimens were cleaned in an ultrasonic bath, degreased with acetone and dried in warm air. Samples of Fe-25Al were pre-oxidized at 1000 °C for 188 h in air in a closed furnace before performing the electrochemical measurements.

Table 2
Electrochemical parameters obtained from potentiodynamic polarization curves of pure Fe in de-aerated 0.5 M H_2SO_4.

E_{corr} V_{SCE}	i_{corr} $\mu A\cdot cm^{-2}$	b_a $V\cdot dec^{-1}$	b_c $mV\cdot dec^{-1}$	Notes	Ref.
−0.50	171	0.10	−0.23	25 °C, scan rate 1 mV/s	[53]
−0.50	410	0.08	−0.11	28 °C, scan rate 0.5 mV/s	[54,55]
−0.48	378	0.04	−0.13	30 °C, scan rate 0.5 mV/s	[56]
−0.51	198	0.06	−0.16	28 °C, scan rate 0.5 mV/s	Present work

Sulphuric acid (H_2SO_4) solution (0.0126 M, pH 1.6) was selected as electrolyte and prepared from concentrated acid and double-distilled water. Before each measurement, the H_2SO_4 solution was de-aerated by flushing with argon (99.999%). The three electrode-method [52] was employed for the electrochemical experiments. A Ag/AgCl reference electrode (6.1243.030, Metrohm) and a platinum foil were adopted as reference and counter electrode, respectively. The temperature of the solution was controlled by a thermostat (E200, Lauda). The reliability of this setup was validated using pure iron as a reference and the results were in very good agreement with literature data [53–56], see Table 2. Prior to performing polarization measurements, the open circuit potential (OCP) was monitored for 60 min. Potentiodynamic polarization curves were determined automatically in the range -1.5 to 2 V with a scan rate of 0.5 mV/s. The OCP and potentiodynamic polarization curves were determined at 25 and 97 °C. These experiments were performed by a computer controlled potentiostat SIMPOT (in-house development of Heinrich-Heine-Universität Düsseldorf). All measurements at 25 and 97 °C were performed for three times in order to confirm reproducibility.

All measured potentials were converted into values against a saturated calomel electrode (SCE). Post mortem examination of the microstructures of the samples were performed by SEM (Gemini 500, Zeiss**)**. To prepare the passive film for XPS analysis, Fe-25Al was passivated in H_2SO_4 (0.0126 M) at 1 V_{SCE} for 300 s after potential sweep from -1.5 to 1 V with a scan rate of 0.5 mV/s. The composition of the passive film was measured by XPS, combined with Ar^+ sputtering for depth profiling using a Physical Electronics PHI Quantera II spectrometer equipped with a monochromatic Al Kα X-ray source (1486.74 eV) and a dual-beam charge neutralizer. The pass energy was set to 140 eV for the survey spectra (energy step 0.2 eV) and 26 eV for high resolution spectra (energy step 0.05 eV). All XP spectra were recorded at a take-off angle of 45°. The measurements were performed in five different areas on the sample surface. For depth profile measurement, the sputtering rate (spot size 2 x 2 μm^2; U = 1 kV) was kept around 3.5 nm/min. Each sputtering cycle lasted for 15 s. XPS data were analyzed by curve fitting using the software CasaXPS [57]. The binding energy scale was referenced to the C − C signal at 284.8 eV. The full width at half maximum (FWHM) of the same components was allowed to vary within a narrow range. Component ratio was determined using CasaXPS embedded

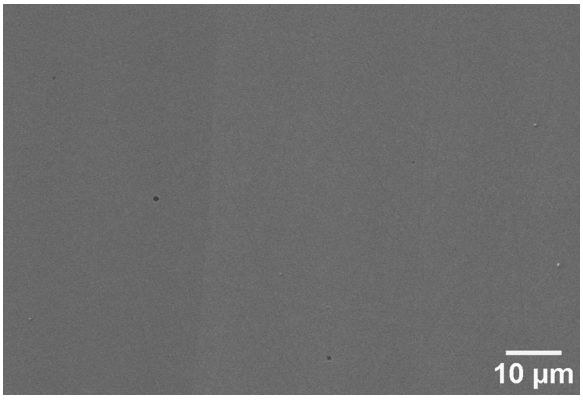

Fig. 1. SEM secondary electron (SE) contrast image of as-cast Fe-40Al.

relative sensitivity factors (RSF) and algorithms. For interpretation, a commonly used online database [58] was used as starting point.

Oxide scales generated by pre-oxidation were characterized by grazing incidence X-ray diffraction (GI-XRD; Seifert ID3003; Co-Kα_1 radiation, λ = 0.178897 nm) with an incidence angle of 2.0° and 2θ steps of 0.05° with a count time of 30 s per step.

3. Results and discussion

Fig. 1 shows the microstructure of as-cast Fe-40Al alloy as an examples. Only very few holes formed during casting can be found and no second phase exists. At 5, 10 and 15 at.% Al the structure is disordered α (Fe,Al) (A2) solid solution, at 25 and 30 at.% Al ordered Fe_3Al ($D0_3$), and at 40 at.% Al ordered FeAl (B2) [59]. The alloys are coarse grained with elongated grains of up to 4 mm width and 10 mm length [60].

3.1. Corrosion behavior at 25 °C

Fig. 2a shows the OCPs of pure Fe, pure Al, and binary Fe-Al alloys in de-aerated H_2SO_4 measured for 3600 s at 25 °C. In addition, the OCP of the stainless steel AISI 304 has been measured for comparison. The OCPs of Fe-Al alloys shifted to more negative values during stabilization with a maximum shift of less than 0.01 V to final values between -0.58 and -0.67 V_{SCE}. With increasing Al content, the OCP of the samples decreased (Fig. 2b). A decrease of the OCP with increasing Al content was also observed in case of Al-Ni alloys [61].

Fig. 3a shows the potentiodynamic polarization curves of pure Fe, pure Al, binary Fe-Al alloys and AISI 304 in de-aerated H_2SO_4. Typical active-passive-transpassive behavior is observed for Fe, AISI 304 and Fe-Al alloys, while pure Al only shows active behavior. Compared with pure Fe, the active dissolution range of the Fe-Al alloys is shifted in the negative direction and lies between that of pure Fe and pure Al. The electrochemical parameters corrosion potential (E_{corr}), corrosion current density (i_{corr}), cathodic Tafel slope (b_c), anodic Tafel slope (b_a), primary passivation potential (E_{pp}), critical passivation current density (i_{crit}), passivation current density (i_{pass}, minimum current density in passivation region), transpassive breakthrough potential (E_b) and width of passive range (E_{pp}-E_b) obtained from the potentiodynamic polarization curves (Fig. 3a) are summarized in Table 3. More specifically, E_{corr}, i_{corr}, b_c and b_a were obtained by fitting the polarization curve in the Tafel region with the Butler-Volmer equation [52], i.e. by four-parameter fitting.

The decrease of E_{corr} with increasing Al content is in accord with the results of the OCP measurements in Fig. 2. The values are also in full agreement with data by Chiang et al. [47], who found a decrease of E_{corr} from -0.59 V_{SCE} for 3.9 at.% Al to -0.65 V_{SCE} for 41.7 at.% Al. In

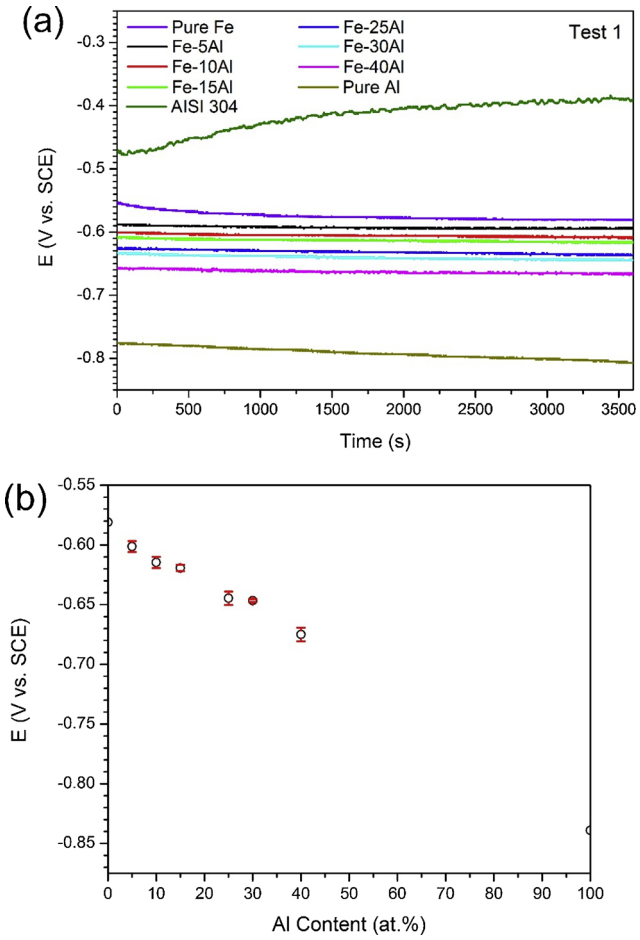

Fig. 2. (a) OCPs of pure Fe, pure Al, stainless steel AISI 304 and binary Fe-Al alloys in de-aerated H_2SO_4 at 25 °C from test series 1 and (b) OCP as a function of Al content.

the present study, the alloys with 5 and 10 at.% Al showed active corrosion behavior (Fig. 3a) while passivation was observed for the alloy with 15 at.% Al and more. By the addition of Al, i_{pass} of Fe-15Al is drastically reduced compared to pure Fe. However, further Al addition does not have much influence on the i_{pass} of the Fe-Al alloys (Table 2). The primary passivation potential E_{pp} still decreases when the Al content is raised to 25 at.%, but does not markedly decrease by further increasing the Al content (Fig. 3b). These results are in reasonable agreement with the observations by Chiang et al. [47], who found that Fe-Al alloys with 10.4 at.% Al and more show passive behavior and no marked decrease in E_{pp} was observed for alloys with an Al content of about 19 at.% or higher. These results are also consistent with the general observation in oxidation experiments that the minimum Al content for the formation of protective Al_2O_3 scales on binary Fe-Al alloys is - depending on temperature - between 12 to 19 at.% [2,62–64]. Such a correlation between aqueous corrosion behavior and oxidation resistance has also been found in case of Fe-Al-C alloys [65]. Though passivation is attained at about 15 at.% Al, the width of the passive range (E_{pp}-E_b) still increases with increasing Al content (Table 3). This observation is again in line with the findings of Chiang et al. [47].

The present results for AISI 304 (Table 3) agree well with those of previous investigations if the differences in the concentration of H_2SO_4 and slight variations in composition are taken into account [66,67]. Compared to the binary Fe-Al alloys, E_{corr} and I_{corr} of AISI 304 are

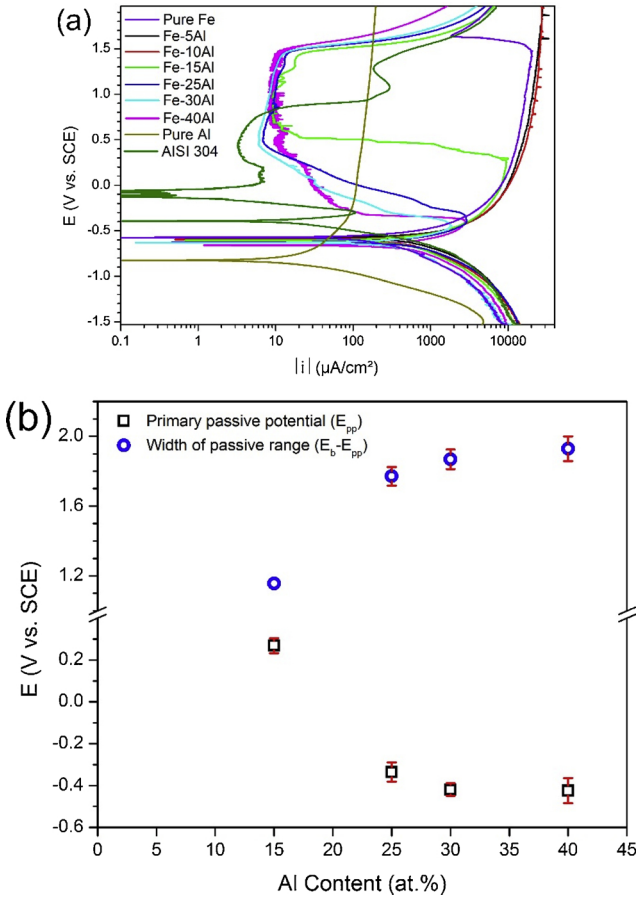

Fig. 3. (a) Potentiodynamic polarization curves of pure Fe, pure Al, stainless steel AISI 304 and binary Fe-Al alloys in de-aerated H_2SO_4 at 25 °C; (b) Primary passivation potential (E_{pp}) and width of passive range (E_b-E_{pp}) as a function of Al content.

improved (Table 3). However, AISI 304 has a narrower passive range compared to the Fe-Al alloys with ≥ 25 at.% Al (Fig. 3a).

The relationship between the passivation behavior of the binary Fe-Al alloys and the Al content is also apparent from the inspection of the sample surfaces after electrochemical testing (Fig. 4). The two alloys with 5 and 10 at.% Al, which did not show passivation during potentiodynamic polarization, were severely corroded. Although Fe-15Al showed passivation during potentiodynamic polarization (Fig. 3a), many big holes were observed on the surface. The alloys with an Al content equal to or higher than 25 at.% preserved flat surfaces, which indicates that the passive film can protect the alloys well from corrosion. This coincides with the observation in Fig. 3 that the increase of Al content does not further improve the corrosion resistance when the Al content exceeds 25 at.%. Some small holes were observed in Fe-25, 30 and 40Al after potentiodynamic polarization (Fig. 4 d–f). Since holes of similar size were also observed in the as-cast alloys (Fig. 1) and impurity contents in these alloys are below levels where second phases form, we conclude that these holes already formed during casting.

3.2. XPS analysis of the passive film

Fig. 5 shows the high resolution XP spectra of Fe $2p_{3/2}$, Al 2p and O 1 s of the passive film of Fe-25Al after 300 s passivation at 1 V_{SCE}. In consistence with literature data [28,65], Al is present as metallic Al (72.4 eV) and Al oxide (74.4 eV). Also, the Fe $2p_{3/2}$ XP spectrum could be fitted with 5 different components. At binding energies of 706.8 and 708.2 eV, the metallic fraction as well as Fe^{2+} are detectable, respectively. The signal of the Fe^{3+} fraction can be divided into three components, Fe-O (711.1 eV), Fe−OH (713.2 eV) and a Fe satellite peak (714.8 eV). These results show that iron oxide is present as mixed oxide and that it co-exists with Al oxide in the passive film. The O 1 s signal was fitted with four components. At lower binding energies, iron oxide (530.52 eV) and iron hydroxide (531.6 eV) could be detected, while Al oxide is present at 532.5 eV. The small peak at 533.7 eV, which was observed in [28], might be attributed to the Al hydroxides [68] (AlOOH, Al(OH), $Al_2O_3{\cdot}H_2O$). However, at the same energy values, it could also represent organic contaminations as well as physisorbed water [69]. The passive film is strongly enriched in Al compared to the bulk alloy composition, which is in consistence with literature [16,18,28,30]. The Al/(Al + Fe) ratio in the passive film is about 55 ± 2. The present value fits to data reported in literature [16,18,28,30] in that the Al/(Al + Fe) ratio of the passive film increases with increasing Al content of the alloy (Table 4). However, the influence of electrolytes and differences in its concentration on this ratio cannot be excluded.

Table 3
Electrochemical parameters obtained from potentiodynamic polarization curves of pure Fe, pure Al and Fe-Al alloys in de-aerated H_2SO_4 (Numbers in bold are average values of 3 measurements).

T °C	Al at. %	OCP V_{SCE}	E_{corr} V_{SCE}	i_{corr} μA/cm²	b_c V·dec⁻¹	b_a V·dec⁻¹	E_{pp} V_{SCE}	i_{crit} μA/cm²	i_{pass} μA/cm²	E_b V_{SCE}	E_p-E_{pp} V_{SCE}
	0	−0.58	−0.57	166	−0.29	0.13	1.48	19661	1835	1.65	0.17
25	5	**−0.60**	**−0.59**	**316**	**−0.32**	**0.13**	–	–	–	–	–
	10	**−0.62**	**−0.58**	**253**	**−0.31**	**0.13**	–	–	–	–	–
	15	**−0.62**	**−0.61**	**431**	**−0.36**	**0.21**	**0.27**	**9687**	–	–	–
	25	**−0.65**	**−0.63**	**447**	**−0.36**	**0.22**	**−0.33**	**3334**	**6.42**	**1.44**	**1.77**
	25*	**−0.63**	**−0.59**	**2.37**	**−0.32**	**0.09**	**−0.45**	**14.78**	**0.33**	**1.46**	**1.91**
	25**	−0.61	−0.60	0.20	−0.16	0.04	−0.43	13.99	0.11	1.59	2.01
	30	**−0.65**	**−0.63**	**387**	**−0.34**	**0.19**	**−0.43**	**2512**	**9.38**	**1.46**	**1.89**
	40	**−0.67**	**−0.67**	**457**	**−0.38**	**0.20**	**−0.34**	**3208**	**22.90**	**1.51**	**1.90**
	100	**−0.84**	**−0.82**	**17**	**−0.18**	**0.50**	–	–	–	–	–
	AISI304	−0.39	−0.39	15	−0.13	0.10	−0.30	107	3.3	1.29	1.60
97	5	**−0.61**	**−0.61**	**1819**	**−0.33**	**0.35**	–	–	–	–	–
	10	**−0.63**	**−0.64**	**1343**	**−0.33**	**0.35**	–	–	–	–	–
	15	**−0.65**	**−0.65**	**1388**	**−0.34**	**0.38**	–	–	–	–	–
	25	**−0.64**	**−0.67**	**1552**	**−0.38**	**0.37**	–	–	–	–	–
	30	**−0.65**	**−0.66**	**1580**	**−0.36**	**0.34**	–	–	–	–	–
	40	**−0.68**	**−0.69**	**806**	**−0.35**	**0.36**	–	–	–	–	–

* Pre-oxidized Fe-25Al.
** Pre-oxidized Fe-25Al after immersing in H_2SO_4 for 308 h before potentiodynamic polarization.

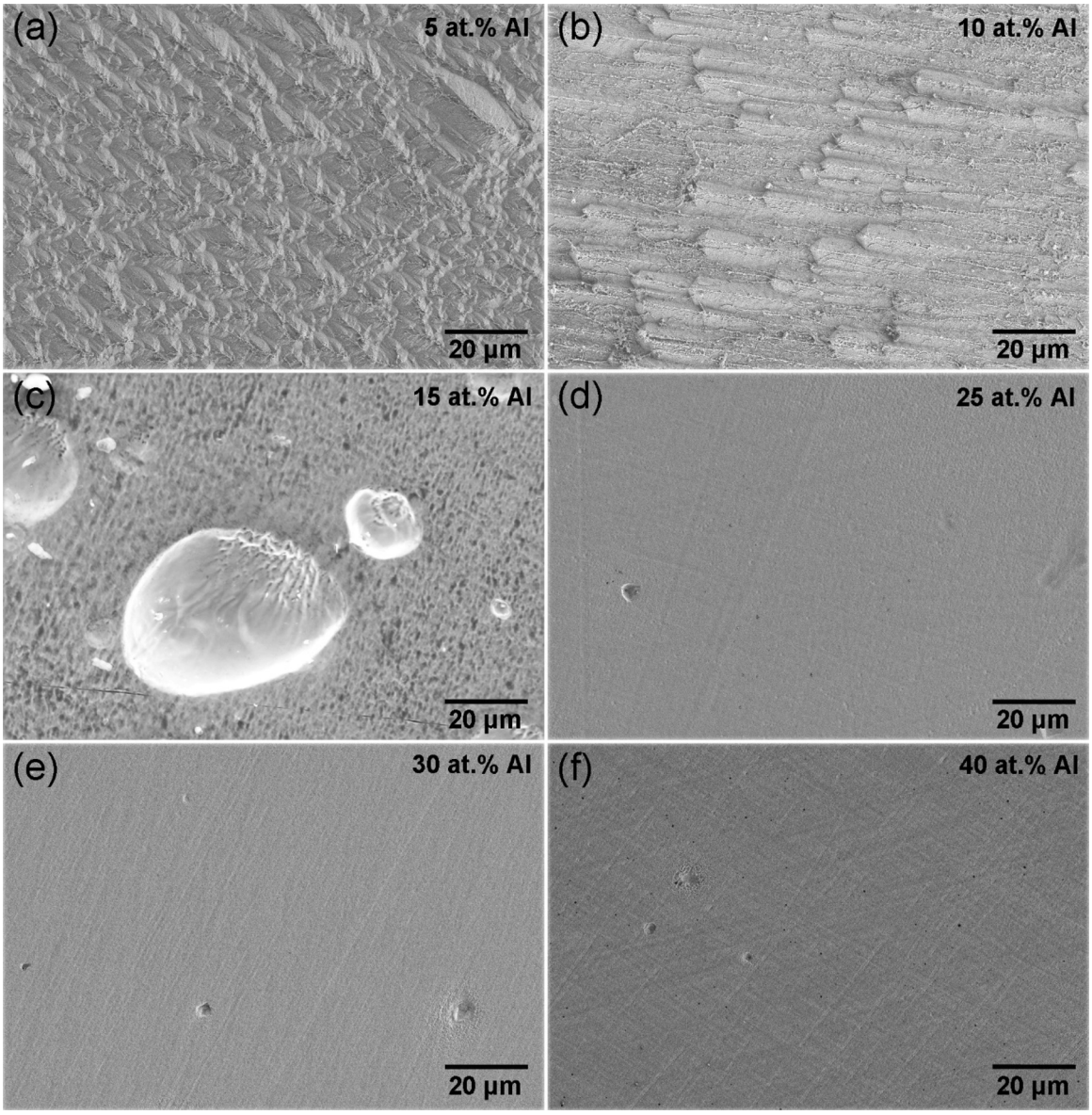

Fig. 4. SEM secondary electron (SE) images of the surfaces of the Fe-Al alloys after the corrosion experiments.

Furthermore, XPS depth profile measurements have been performed and qualitatively analyzed. Fig. 6 shows the comparison of the surface spectrum and spectra obtained after subsequent sputtering cycles. After the first sputtering cycle, the Fe, Al and O peaks increase which is due to the removal of contamination from the surface. After the second and third sputtering cycles, the signal attributed to oxide in the Fe $2p_{3/2}$ spectrum decreases more and more and is not detectable anymore after the fourth sputtering cycle. No significant changes are visible in the Al 2p spectrum from the first to the third sputtering cycle, but exactly after the fourth sputtering cycle, where the iron oxide peak is not any longer seen, the higher binding Al 2p component attributed to the Al^{3+} shifts towards even higher binding energies, likewise the O 1 s peak. The metallic Fe 2p and Al 2p peaks do not show any shift in their position throughout the sputtering process. Upon further sputtering, the Al^{3+} and O signals are further decreasing and the Al^{3+} peak position is slowly shifting back towards its initial position. The alumina in greater depth is certainly mainly internal oxide and does not comprise a closed layer anymore, as otherwise the metallic components at the surface would be too high.

Assuming that the passive film on Fe-25Al hence consists mainly of the mixed Fe and Al oxide layer with a very thin alumina layer underneath, which might be the region where the mentioned peak shift is measured, the thickness will be about 8 nm, which is slightly larger than values reported in literature (5 nm [28,30], ˜4 nm [16]). However, differences in alloy compositions and electrolytes used in [16,28,30] may explain this discrepancy.

Regarding the structure of the passive film, three models were proposed so far in the literature. Schaepers et al. [19] proposed a sandwich-like structure where an Al oxide enriched zone in the center of the passive film is wrapped by two layers consisting of a mixture of Al and Fe oxides. Frangini et al. [28] thought that the passive film consisted of two layers. An outer layer of mixed aluminium-iron oxyhydroxide and an inner layer composed mostly of an aluminium-rich oxide phase. Shankar Rao [48] proposed that the passive film is a single

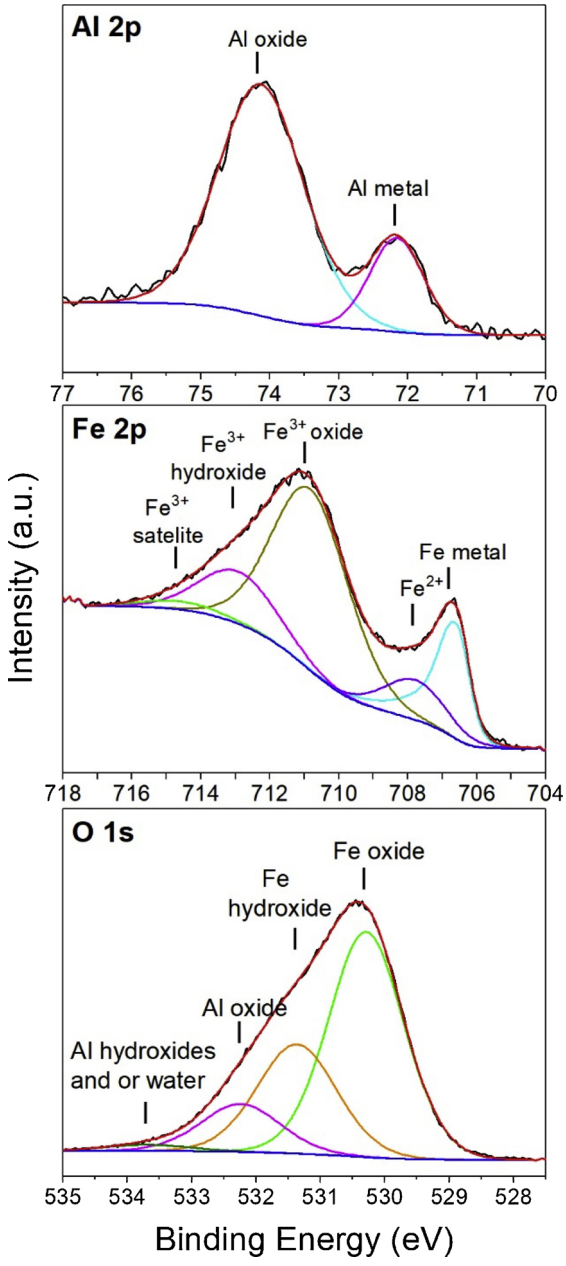

Fig. 5. High resolution XP spectra of Al 2p, Fe 2p and O 1 s of the passive film of Fe-25Al after 300 s passivation at 1 V_{SCE} with background subtraction and curve fitting.

layer comprised out of a mixture of Al and Fe oxides. The present XPS measurements of the passive film confirm the general findings that (i) the passive film is enriched in Al in the form of Al^{3+} compared to the bulk alloy and (ii) coexistence of Al and Fe oxides in the film [48]. Concerning the structure, the depth resolved XPS spectra obtained here (Fig. 6) indicate a structure similar to the one proposed by Frangini et al. [28]. However, the alumina layer beneath the mixed layer of aluminium-iron oxy-hydroxide will have to be very thin and might have a yet unknown special structure that is correlated to the observed peak shift.

As it has been shown that the formation of the passive film very much depends on the Al content of the bulk alloy, the electrolyte, the applied potential, the time dependent evolution of the passive film and other factors [19,28,29,46,48], differences in the structure of the passive film may be related to such variances.

Table 4
Al/(Al + Fe) ratio in the passive film that formed on different binary Fe-Al alloys during electrochemical testing.

Alloys (in at.%)	Al/(Al + Fe) ratio	Electrolyte and pH	References
Fe-6Al	0.30	0.5 M H_2SO_4	[18]
Fe-8Al	0.22	0.1 M phthalate buffer, pH	[16]
Fe-15Al	0.35	5	
Fe-22Al	0.38		
Fe-25Al	0.55	0.0126 M H_2SO_4, pH 1.6	Present study
Fe-40Al	0.70	0.5 M H_2SO_4	[28]

3.3. Corrosion behavior at 97 °C

The OCPs and potentiodynamic polarization curves of the binary Fe-Al alloys in de-aerated H_2SO_4 were also determined at 97 °C (Fig. 7) and the electrochemical parameters are summarized in Table 3. Similar to the results at 25 °C, the OCP at 97 °C decreases with increasing Al content. All OCPs are lower than at 25 °C for the same alloy. None of the alloys shows passive behavior at 97 °C. For all alloys, the corrosion current densities are two to four times higher at 97 °C than at 25 °C.

3.4. Effect of pre-oxidation

Since the passive film mainly consists of oxide, it is meaningful to investigate, whether formation of an oxide scale by pre-oxidation can increase the corrosion resistance of Fe-Al. Fig. 8 shows the surface, cross section and GI-XRD pattern of Fe-25Al after oxidation at 1000 °C for 188 h in air. A dense and uniform oxide layer of about 1.5 µm thickness has formed. The oxide layer has very good adherence to the substrate. No cracking and scale spallation are observed after cooling to room temperature. GI-XRD analysis indicates that the oxide layer consists mainly of α-Al_2O_3 with a small amount of $FeAl_2O_4$ spinel. This is consistent with previous investigations, which showed that on Fe-25Al oxidized at 1000 °C predominantly α-Al_2O_3 forms [2,51,62,70]. The formation of $FeAl_2O_4$ here may be due to the lower partial pressure of oxygen in the closed furnace than in flowing air.

The potentiodynamic polarization curves of Fe-25Al with and without pre-oxidation in de-aerated H_2SO_4 are shown in Fig. 9a and the corresponding electrochemical parameters are listed in Table 3. Because the current densities in the passivation range in two of the three measurements are below the resolution limit of the instrument, broad signals are observed in the passive range for the pre-oxidized alloy. For the pre-oxidized alloy, all electrochemical parameters are close to each other, or at least in the same order of magnitude, except i_{pass}. This difference may be attributed to the different surface conditions of the pre-oxidized samples. However, i_{corr}, i_{crit} and i_{pass} of the pre-oxidized alloy are still significantly smaller than those for the alloy without pre-oxidation. More specifically, i_{corr} and i_{crit} of the pre-oxidized alloy are two orders of magnitude smaller than without pre-oxidation and i_{pass} is one order of magnitude smaller. This reveals that the oxide layer generated by pre-oxidation can well protect Fe-25 at.% Al from corrosion. Fig. 9b shows the surface of the pre-oxidized alloy after the polarization measurement. The oxide scale is intact and its appearance resembles that of the scale before the test (Fig. 8a).

To study the protectiveness of the oxide scale during prolonged aqueous corrosion, pre-oxidized Fe-25Al was tested in the passive range at 1 V_{SCE} for 70 h (Fig. 10). For about 10 h, i_{pass} remains constant,

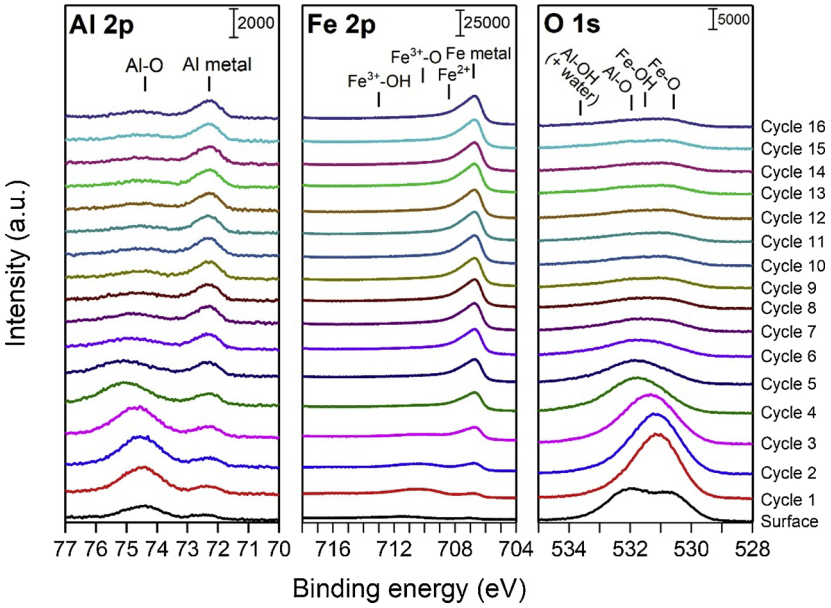

Fig. 6. Comparison of the surface spectrum and spectra of the obtained after subsequent sputtering cycles.

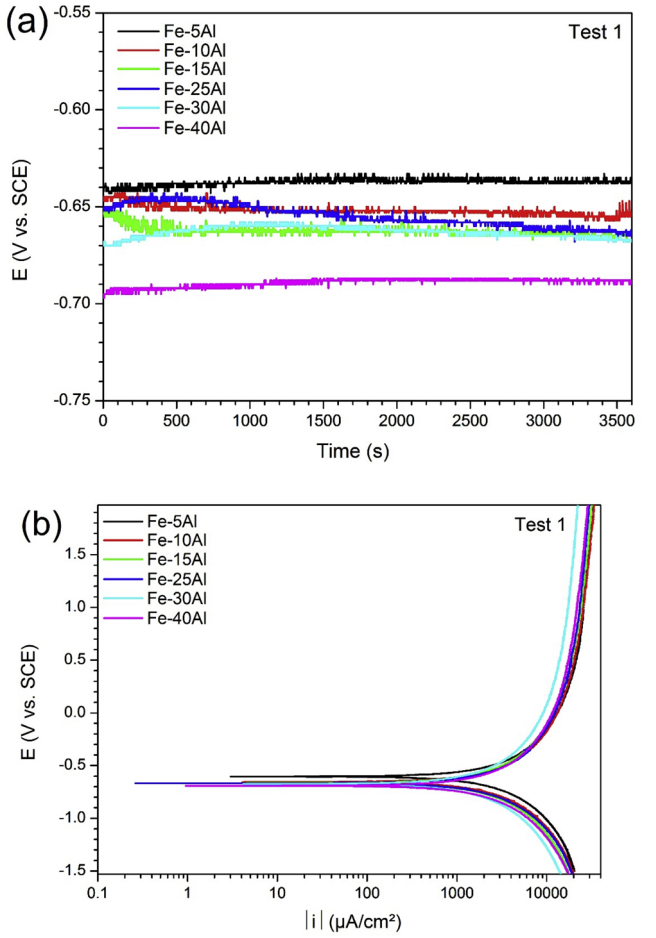

Fig. 7. (a) OCPs and (b) potentiodynamic polarization curves of binary Fe-Al alloys at 97 °C.

before it starts to increase, indicating increased corrosion. i_{pass} increases further, but after about 30 h it goes back to the original value, where it stays until the end of the test. Apparently, there is some, at least partial or localized, break down of the protecting oxide scale. However, the alloy quickly re-passivates and i_{pass} even goes back to the value of the pre-oxidized alloy which is about one magnitude lower than that of the alloy without pre-oxidation. Quick re-passivation after scratching has also been observed in case of an Fe_3Al-based alloy [41]. This indicates that the observed break-down was only very localized, as otherwise it is not conceivable how the current density in the passive range could be so low. But even the fact that re-passivation of localized defects is possible is remarkable and shows that the matrix below the scale is not too significantly depleted from metallic aluminum.

For further evaluation of the stability of the oxide layer, pre-oxidized Fe-25Al was immersed in H_2SO_4 for 308 h before potentiodynamic polarization (Fig. 9a). Even after such a long immersion, the morphology of the surface is almost the same as before and no obvious dissolution of the oxide layer can be observed. Moreover, the polarization curve does not show any marked effects (Fig. 9a). The above results show the formed oxide scale is quite stable during aqueous corrosion and that can well protect the Fe-25Al from corrosion.

The good corrosion resistance of pre-oxidized Fe-Al observed in the present study is attributed to the following three reasons: Firstly, the studied Fe-25Al alloy is single-phase without any defects, such as second phases, oxides, segregations or local enrichment, which is beneficial for forming a dense, uniform and continuous oxide layer. Secondly, the pre-oxidation treatment employed here was sufficiently long and at suitable high temperature for the formation of a protective oxide scale. Thirdly, using the Scherrer equation [71], the average grain size of $FeAl_2O_4$ spinel is determined to be about 150 nm. This nanosized $FeAl_2O_4$ in α-Al_2O_3 may refine the structure of the oxide layer and perhaps restrict the passage of ions through the oxide layer and protect the substrate from corrosion [72].

4. Conclusions

At 25 and 97 °C, the OCP of Fe-Al alloys with Al contents between 0 and 40 at.% Al decreases with increasing Al content. The minimum Al content for the formation of a passive layer on binary Fe-Al in 0.0126 M H_2SO_4 at 25 °C is about 15 at %. The alloy with 25 at.% Al shows even better passivation, but no marked improvement is revealed when the Al content increases to 40 at.%. At 97 °C, none of the alloys shows passive behavior. Post-mortem examination of the samples corresponds with these results, in that the alloys with 5 and 10 at.% Al, which showed only active corrosion, showed a strong corrosive attack. XPS

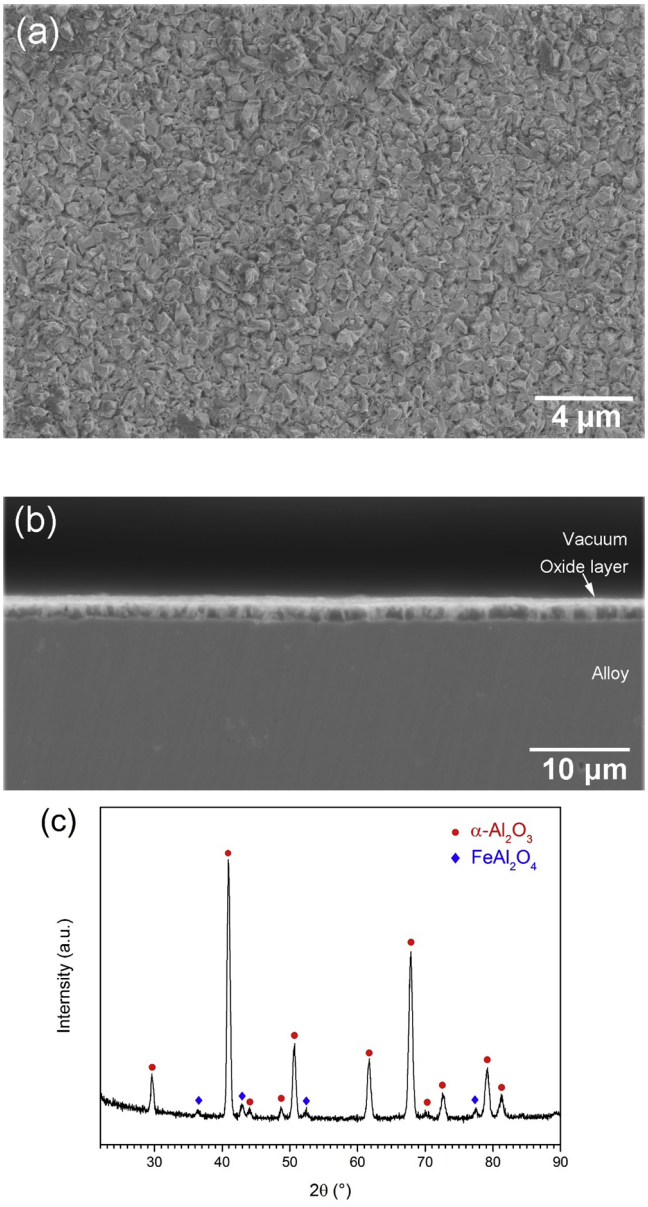

Fig. 8. SEM-SE images of the (a) surface, (b) cross section and (c) GI-XRD pattern of Fe-25Al after oxidation at 1000 °C for 188 h in air.

measurements of the passive film reveal a strong Al enrichment compared to the bulk alloy. The passivation of Fe-Al alloys is related to the formation of a passive film consisting of a mixture of Fe and Al oxides, possibly with a thin layer of alumina underneath. That for Fe-Al such a passive range is observed, which was not found for pure Al, indicates that the passive layer seems to have a special, very stable structure. This is an object of further investigations.

A dense, uniform and continuous oxide scale formed on Fe-25Al after oxidation in air at 1000 °C for 188 h. The present results for the first time conclusively show that pre-oxidation can substantially improve the aqueous corrosion behavior of Fe-Al alloys. This point had been disputed before. It has also been shown that re-passivation occurred in the pre-oxidized samples in case of failure at small defects and that long-time immersion of the scale has no effect on its beneficial performance, because the formed scale seems to be surprisingly stable. In fact during the investigated time no measurable loss of scale was observed. It could be that the presence of nanoscaled spinel in the scale might play a role here.

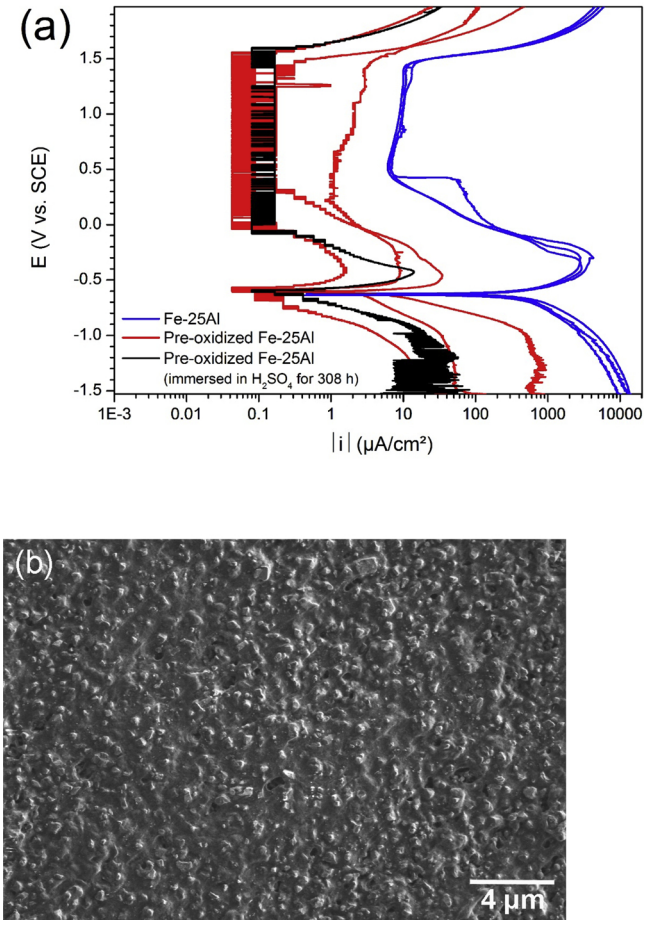

Fig. 9. (a) Potentiodynamic polarization curves of Fe-25Al with and without pre-oxidation in de-aerated H_2SO_4 at 25 °C. (b) SEM-SE micrograph of the surface of pre-oxidized Fe-25Al after the polarization measurement.

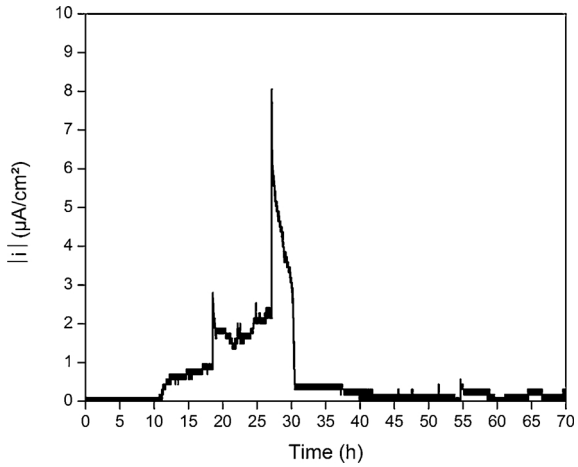

Fig. 10. Current density decay of pre-oxidized Fe-25Al in de-aerated H_2SO_4 at an applied anodic potential of 1 V_{SCE}.

Data availability

The raw/processed data required to reproduce these findings cannot be shared at this time due to time limitations.

Acknowledgements

The authors would like to thank Mr. B. Breitbach for GI-XRD

measurement, Mr. T. Wickfeld and Mr. M. Bütow for EDM preparation of the samples. Partial financial support by the European Union's research and innovation program Horizon 2020 under grant No 634135 is gratefully acknowledged.

References

[1] E.M. Savitskii, V.F. Terekhova, I.V. Burov, Effect of certain less common alloying elements on the mechanical properties of iron-aluminum alloys, Met. Sci. Heat Treat. 1 (1959) 43–50.
[2] P. Tomaszewicz, G.R. Wallwork, Iron-Aluminum alloys: a review of their oxidation behavior, Rev. High Temp. Mater. 4 (1978) 75–104.
[3] N.S. Stoloff, Iron aluminides: present status and future prospects, Mater. Sci. Eng. A 258 (1998) 1–14.
[4] C.G. McKamey, Iron aluminides, in: N.S. Stoloff, V.K. Sikka (Eds.), Physical Metallurgy and Processing of Intermetallic Compounds, Chapman & Hall, New York, 1996, p. 351.
[5] D.G. Morris, M.A. Munoz-Morris, Recent developments toward the application of iron aluminides in fossil fuel technologies, Adv. Eng. Mater. 13 (2011) 43–47.
[6] J.F. Nachman, E.R. Duffy, Effect of alloying additions on sea water corrosion resistance of iron-aluminum base alloys, Corrosion 30 (1974) 357–365.
[7] C.T. Liu, E.P. George, P.J. Maziasz, J.H. Schneibel, Recent advances in B2 iron aluminide alloys: deformation, fracture and alloy design, Mater. Sci. Eng. A 258 (1998) 84–98.
[8] P.J. Blau, H.M. Meyer III, Characteristics of wear particles produced during friction tests of conventional and unconventional disc brake materials, Wear 255 (2003) 1261–1269.
[9] R. Schulz, S. Savoie, A new family of high performance nanostructured catalysts for the electrosynthesis of sodium chlorate, J. Alloys. Compd. 483 (2009) 510–513.
[10] J.E. Flores-Chan, A. Torres-Islas, C. Patiño-Carachure, G. Rosas, M.A. Espinosa-Medina, Corrosion study of Al-Fe (20 wt%) alloy in seawater alkaline solutions, Int. J. Electrochem. Sci. 11 (2016) 7359–7369.
[11] G. Sharma, P.R. Singh, R.K. Sharma, K.B. Gaonkar, R.V. Ramanujan, Aqueous corrosion behavior of iron aluminide intermetallics, J. Mater. Eng. Perform. 16 (2007) 779–783.
[12] W.-C. Luu, W.-C. Chiang, J.-K. Wu, Effect of Cr and Ti additions on the corrosion behavior of Fe_3Al alloys in chloride-containing sulfuric acid solutions, Mater. Lett. 59 (2005) 3295–3298.
[13] T.N. Kutz, D. Zander, The Influence of chromium on the passivation of Fe_3Al iron aluminides, investigated via potentiodynamic polarization in 0.25 M H_2SO_4, Corrosion 73 (2017) 648–654.
[14] F. Rosalbino, R. Carlini, R. Parodi, G. Zanicchi, G. Scavino, Investigation of passivity and its breakdown on Fe_3Al-Si and Fe_3Al-Ge intermetallics in chloride-containing solution, Corros. Sci. 85 (2014) 394–400.
[15] A. Agarwal, M.J. Akhtar, R. Balasubramaniam, Effect of alloying on aqueous corrosion and mechanical behaviour of iron aluminide Fe_3AI, J. Mat. Sci. 31 (1996) 5207–5213.
[16] D. Schaepers, H.-H. Strehblow, Surface analytical investigations of electrochemically formed passive layers on binary Fe/Al alloys, J. Electrochem. Soc. 142 (1995) 2210–2218.
[17] D. Schaepers, H.-H. Strehblow, An XPS and ISS investigation of passive layers on binary Fe-Al alloys, Corros. Sci. 39 (1997) 2193–2213.
[18] R. Kirchheim, B. Heine, S. Hofmann, H. Hofsäss, Compositional changes of passive films due to different transport rates and preferential dissolution, Corros. Sci. 31 (1990) 573–578.
[19] D. Schaepers, H.-H. Strehblow, U. Künzelmann, Y. Schwarz, Electrochemical, ellipsometrical and surface analytical investigations of passive layers on binary Fe/Al alloys, Surf. Interface Anal. 21 (1994) 342–348.
[20] B. Łosiewicza, A. Budniok, M. Freitag, M. Kupka, Structure and electrochemical corrosion resistance of the passivated Fe-40 at.% Al binary alloy in sulfuric acid solution, Solid State Phenom. 163 (2010) 68–71.
[21] A. Torres-Islas, C. Carachure, S. Serna, B. Campillo, G. Rosas, Corrosion of mechanically alloyed nanostructured FeAl, Adv. Mater. Sci. Eng. Int. J. (2012) 1–9, https://doi.org/10.1155/2012/629802.
[22] E. Huape-Padilla, M. Sánchez-Carrillo, J.P. Flores-de los Rios, M.A. Espinosa-Medina, R.G. Bautista-Margulis, M.I. Ferrer-Sánchez, G. Carbajal-de la Torre, L. Bejar-Gómez, J.G. Chacón-Nava, A. Martínez-Villafañe, Corrosion study of Fe-Al intermetallic alloys in simulated acid rain, Int. J. Electrochem. Sci. 10 (2015) 2141–2154.
[23] E. Karapanou, A.G. Lekatou, A.K. Sfikas, E. Georgatis, K. Lentzaris, A.E. Karantzalis, Vacuum arc melting processed Fe-Al matrix based intermetallic composites, reinforced with VC phases: assessment of microstructure, sliding wear and aqueous corrosion response, Mater. Sci. Eng. Adv. Res. Special (2017) 1–6, https://doi.org/10.24218/msear.2017.1S.
[24] F. Rosalbinoa, R. Carlini, R. Parodi, G. Zanicchi, Effect of silicon and germanium alloying additions on the passivation characteristics of Fe_3Al intermetallic in sulphuric acid solution, Electrochim. Acta 62 (2012) 305–312.
[25] F. Rosalbino, R. Carlini, G. Zanicchi, G. Scavino, Effect of copper alloying addition on the electrochemical corrosion behaviour of Fe_3Al intermetallic in sulphuric acid solution, Mater. Corros. 67 (2016) 1042–1048.
[26] P. Brito, É. Schuller, J. Silva, T.R. Campos, C.R. de Araújo, J.R. Carneiro, Electrochemical corrosion behaviour of (100), (110) and (111) Fe_3Al single crystals in sulphuric acid, Corros. Sci. 126 (2017) 366–373.
[27] H.C. Choe, H.S. Kim, D.C. Choi, K.H. Kim, Effects of alloying elements on the electrochemical characteristics of iron aluminides, J. Mater. Sci. 32 (1997) 1221–1227.
[28] S. Frangini, N. De Cristofaro, A. Mignone, J. Lascovich, R. Giorgi, A combined electrochemical and XPS study on the passivity of B2 iron aluminides in sulphuric acid solution, Corros. Sci. 39 (1997) 1431–1442.
[29] S. Frangini, N. De Cristofaro, J. Lascovich, A. Mignone, On the passivation characteristics of a β-FeAl intermetallic compound in sulphate solutions, Corros. Sci. 35 (1993) 153–159.
[30] S. Frangini, R. Giorgi, J. Lascovich, A. Mignone, XPS study of passive films formed on an iron-aluminium intermetallic compound in acid solution, Surf. Interface Anal. 21 (1994) 435–441.
[31] N. De Cristofaro, S. Frangini, A. Mignone, Passivity and passivity breakdown on a β-FeAl intermetallic compound in sulphate and chloride containing solutions, Corros. Sci. 38 (1996) 307–315.
[32] S. Frangini, J. Lascovich, AC impedance study of passive B2 FeAl intermetallic alloy in sulphuric acid, Electrochim. Acta 40 (1995) 637–642.
[33] S. Frangini, Corrosion rate and anodic dissolution behavior of a B2-iron aluminide alloy in sulfuric acid, Corrosion 55 (1999) 89–95.
[34] S. Frangini, J. Lascovich, N. De Cristofaro, Pitting susceptibility of chromium modified passive films of a B2-FeAl intermetallic alloy, Mater. Sci. Forum 185-188 (1995) 1041–1048.
[35] J.N. Defrancq, Cast iron with high Al-content in sulfuric acid, Mater. Corros. 28 (1977) 480–483.
[36] Y.-S. Choi, J.-G. Kim, Investigation of passivity and its breakdown on Fe_3Al-Cr-Mo intermetallics in thiosulfate-chloride solution, Mater. Sci. Eng. A 333 (2002) 336–342.
[37] A.K. Nigam, R. Balasubramaniam, S. Bhargava, R.G. Baligidad, Electrochemical impedance spectroscopy and cyclic voltammetry study of carbon-alloyed iron aluminides in sulfuric acid, Corros. Sci. 48 (2006) 1666–1678.
[38] B.W. Madsen, T.A. Adler, Passivation and repassivation kinetics of iron-aluminum alloys in 1 N H_2SO_4 using potential step and scratch tests, Wear 171 (1994) 215–225.
[39] J.G. Kim, R.A. Buchanan, Pitting and crevice corrosion of iron aluminides in a mild acid-chloride solution, Corrosion 50 (1994) 658–668.
[40] M.C. Garcıa-Alonso, M.F. Lopez, M.L. Escudero, J.L. González-Carrasco, D.G. Morris, Corrosion behaviour of an Fe_3Al-type intermetallic in a chloride containing solution, Intermetallics 7 (1999) 185–191.
[41] V. Shankar Rao, Repassivation behaviour and surface analysis of Fe_3Al based iron aluminide in 0.25 M H_2SO_4, Corros. Sci. 47 (2005) 183–194.
[42] S. Sriram, R. Balasubramaniam, M.N. Mungole, S. Bharagava, R.G. Baligidad, Effect of cerium addition on the corrosion behaviour of carbon-alloyed iron aluminides, Corros. Sci. 48 (2006) 1059–1074.
[43] R.A. Buchanan, R.L. Perrin, Effects 1000 °C oxide surfaces on room temperature aqueous corrosion and environmental embrittlement of iron aluminides, in: R.R. Judkins (Ed.), 11th Annu. Conf. on Fossil Energy Materials, Oak Ridge National Laboratory (1997) 159–168.
[44] M.F. Lopez, M.L. Escudero, Corrosion behaviour of FeAl-type intermetallic compounds, Electrochim. Acta 43 (1998) 671–678.
[45] M.L. Escudero, M.C. Garcia-Alonso, J.L. Gonzalez-Carrasco, M.A. Munoz-Morris, M.A. Montealegre, C. Garcia Oca, D.G. Morris, S.C. Deevi, Possibilities for improving the corrosion resistance of Fe-40Al intermetallic strip by prior oxide protection, Scr. Mater. 48 (2003) 1549–1554.
[46] N. Masahashi, G. Kimura, M. Oku, K. Komatsu, S. Watanabe, S. Hanada, Corrosion behavior of iron-aluminum alloys and its composite steel in sulfuric acid, Corros. Sci. 48 (2006) 829–839.
[47] W.-C. Chiang, W.-C. Luu, J.-K. Wu, Effect of aluminum content on the passivation behavior of Fe-Al alloys in sulfuric acid solution, J. Mater. Sci. 41 (2006) 3041–3044.
[48] V. Shankar Rao, A review of the electrochemical corrosion behaviour of iron aluminides, Electrochim. Acta 49 (2004) 4533–4542.
[49] P.F. Tortorelli, J.H. DeVan, Behavior of iron aluminides in oxidizing and oxidizing/sulfidizing environments, Mater. Sci. Eng. A 153 (1992) 573–577.
[50] F. Lang, Z. Yu, S. Gedevanishvilic, S.C. Deevid, T. Narita, Effect of pre-oxidation on the corrosion behavior of Fe-40Al sheet in a N_2-11.2O_2-7.5CO_2-500 ppm SO_2 atmosphere at 1273 K, Intermetallics 11 (2003) 129–134.
[51] A.Y. Ilyushechkin, M.D. Dolan, K.G. McLennan, S.D. Sharma, Effect of pre-oxidation of Fe_3Al on its corrosion resistance in sulfur and chlorine contaminated syngas, Asia-Pac, J. Chem. Eng. 7 (2011) 716–725.
[52] N. Perez, Electrochemistry and Corrosion Science, Kluwer Academic Publishers, Boston, 2004.
[53] K.F. Khaled, N. Hackerman, Investigation of the inhibitive effect of ortho-substituted anilines on corrosion of iron in 0.5 M H_2SO_4 solutions, Mater. Chem. Phys. 82 (2003) 949–960.
[54] C. Jeyaprabha, S. Sathiyanarayanan, S. Muralidharan, G. Venkatachari, Corrosion inhibition of iron in 0.5 mol L^{-1} H_2SO_4 by halide ions, J. Brazil Chem. Soc. 17 (2006) 61–67.
[55] C. Jeyaprabha, S. Sathiyanarayanan, G. Venkatachari, Corrosion inhibition of pure iron in 0.5M H_2SO_4 solutions by ethanolamines, Appl. Surf. Sci. 246 (2005) 108–116.
[56] S.A. Umoren, Y. Li, F.H. Wang, Electrochemical study of corrosion inhibition and adsorption behaviour for pure iron by polyacrylamide in H_2SO_4: synergistic effect of iodide ions, Corros. Sci. 52 (2010) 1777–1786.
[57] N. Fairley, CasaXPS VAMAS Processing Software, available at (2010) http://www.casaxps.com.
[58] http://xpssimplified.com/elements, Accessed May 23, 2018.
[59] D. Risanti, J. Deges, L. Falat, S. Kobayashi, J. Konrad, M. Palm, B. Pöter,

A. Schneider, C. Stallybrass, F. Stein, Dependence of the brittle-to-ductile transition temperature (BDTT) on the Al content of Fe-Al alloys, Intermetallics 13 (2005) 1337–1342.
[60] F. Stein, M. Palm, Re-determination of transition temperatures in the Fe-Al system by differential thermal analysis, Int. J. Mater. Res. 98 (2007) 580–588.
[61] C. Xu, L. Du, B. Yang, W. Zhang, The effect of Al content on the galvanic corrosion behaviour of coupled Ni/graphite and Ni-Al coatings, Corros. Sci. 53 (2011) 2066–2074.
[62] R. Prescott, M.J. Graham, The oxidation of iron-aluminum alloys, Oxid. Met. 38 (1992) 73–87.
[63] I. Rommerskirchen, B. Eltester, H.J. Grabke, Oxidation of β-FeAl and Fe-Al alloys, Mater. Corros. 47 (1996) 646–649.
[64] V. Marx, M. Palm, Oxidation of Fe-Al Alloys (5-40 at.% Al) at 700 and 900 °C, Mater. Sci. Forum 879 (2016) 1245–1250.
[65] V. Shankar Rao, V.S. Raja, Correlation between high-temperature oxidation and electrochemical corrosion behavior in sulfuric acid of Fe-Al-C alloys: an insight, Corrosion 6 (2005) 751–756.
[66] A. Pardo, M.C. Merino, M. Carboneras, F. Viejo, R. Arrabal, J. Muñoz, Influence of Cu and Sn content in the corrosion of AISI 304 and 316 stainless steels in H_2SO_4, Corros. Sci. 48 (2006) 1075–1092.
[67] A. Pardo, M.C. Merino, A.E. Coy, F. Viejo, R. Arrabal, E. Matykina, Effect of Mo and Mn additions on the corrosion behaviour of AISI 304 and 316 stainless steels in H_2SO_4, Corros. Sci. 50 (2008) 780–794.
[68] B.R. Strohmeier, Surface characterization of aluminum foil annealed in the presence of ammonium fluoborate, Appl. Surf. Sci. 40 (1989) 249–263.
[69] I. Olefjord, H. Mathieu, P. Marcus, Intercomparison of surface analysis of thin aluminium oxide films, Surf. Interface Anal. 15 (1990) 681–692.
[70] D. Das, R. Balasubramaniam, M.N. Mungole, Hot corrosion of Fe_3Al, J. Mater. Sci. 37 (2002) 1135–1142.
[71] P. Scherrer, Nachr Ges wiss goettingen, Math. Phys. 2 (1918) 98–100.
[72] X.H. Chen, J.H. Dong, E.H. Han, W. Ke, Effect of Al alloying on corrosion performance of steel, Corros. Eng. Sci. Technol. 42 (2007) 224–231.